Defence Science Journal, Vol. 72, No. 4, July 2022, pp. 600-608, DOI : 10.14429/dsj.72.17658

Comparative Study of Microstructural, Mechanical and Electrochemical Aspects of As-Deposited and Shock Wave Exposed Ni-W Nanostructured Coatings

G. Nivetha,[#] R. Kannan,[$,*] M. Selvambikai,[#] C. Vasantharaj,[%] B. Praveen Kumar,[^] P.S. Premkumar[#] and K. Sundararaj[#]

[#]*Kumaraguru College of Technology, Coimbatore, Tamil Nadu – 641 049, India*
[%]*Kumaraguru Centre for Industrial Research and Innovations (KCIRI), Coimbatore, Tamil Nadu - 641 049, India*
[^]*DRDO - Armament Research & Development Establishment (ARDE), Pune, Maharashtra - 411021, India*
[*]*Email: kannan.r.sci@kct.ac.in*

ABSTRACT

The current work describes the effect of shock wave exposure on electroplated NiW (Nickel – Tungsten) coatings. NiW coatings were deposited by varying the bath temperatures (35 °C and 75 °C) at a constant current density of 1A/dm^2. The deposited NiW thin films were exposed to shock waves with varying Mach numbers of 1.34 and 2.33 using an in-house shock wave tube facility. The as-deposited and shock wave-exposed NiW coatings were characterized by XRD (X-ray Diffraction), FESEM (Field Emission Scanning Electron Microscope), EDS (Energy Dispersive X-ray spectroscopy), Vickers micro indenter, Pin-on-disc and EIS (Electrochemical Impedance Spectroscopy) to reveal its structural and mechanical properties. The XRD results disclose the stable cubic (Face Centred Cubic) structural phase of as deposited and shock wave exposed NiW coatings with average crystallite size varying between 5 nm to 17nm. The elemental composition of as deposited and shockwave exposed coatings are similar as confirmed in the EDS analysis. This henceforth represents the stability of nanostructured NiW coating in terms of compositional and structural aspects. Morphological analysis through FESEM shows that the exposed thin film is defect-free due to the impact of shock waves. Furthermore, corrosion resistance is observed to enhance ten times in shockwave exposed thin film than in as-deposited thin film for a higher Mach number (Pressure ~63 bar). Similarly, corrosion resistance for low Mach number (pressure ~13 bar) increases by three times of as-deposited film according to the EIS analysis. Therefore, the structural, morphological and corrosion properties were enhanced upon surface treatment by shock wave exposure.

Keywords: Surface treatment; NiW; Electrodeposition; Corrosion rate; Shock tube; Mach number

1. INTRODUCTION

Protective coatings have been deposited using various methodologies and widely classified into various categories. Among these electrodepositions is one of the most suitable chemical techniques where the bath solution is prepared and through the application of an electric current between electrodes, the coating is being deposited. Electrodeposition coatings are mostly used for the deposition of metal-based alloys. Bi-metal alloys and tri-metal alloys were coated using electrodeposition. The electrodeposition method is widely used in industrial-scale applications for the deposition of metals such as gold, silver and so The electrodeposition technique on an industrial scale is known as the electroplating process. Therefore, the electrodeposition pross is simple and user-friendly, but the main requirement of the electrodeposition process is that the base specimen used should be conductive.[1] The existence of Nano-structuring in the thin film leads to improved mechanical properties such as improved hardness, wear and corrosion resistance.

Received : 12 November 2021, Revised : 14 April 2022
Accepted : 30 June 2022, Online published : 26 August 2022

Nickel-based alloys have been widely studied and used in industrial applications owing to their corrosion resistance and improved mechanical properties when compared to other alloys as protective coatings. Nickel-based alloys have been proven to exhibit high temperature and pressure resistance used in applications such as pipes used for drilling. In contrast, nickel-based alloys have proven to be resistant to a few chemical components such H_2S, CO_2, and chlorides.[2] These alloys are used in other applications such as aircraft, rocket engines, submarines, marine turbines, and vehicular turbines. The alloys are marketed under various names such as Waspaloy, M-252, Nimonoic 105, Nimonic 115, Rene 41, and 95. The wider aspect of nickel alloying elements are aluminum, titanium, niobium, silicon, molybdenum, cobalt, tungsten, chromium, and many other such materials. Alloy matrix elements play a vital role in the resulting material properties.[3]

Srivastava,[4] *et al.* deposited nickel-cobalt alloys by electrodeposition by varying the cobalt concentration. The cobalt-rich alloy showed poor corrosion protection compared to the 20 % Ni-Co alloy.[4] Another group Allahyarzadeh, *et al.* investigated electrodeposited NiW alloy coatings and found them to be exhibited better corrosion and wear resistance.[5] Various alloys were investigated both iatthe nanoscale and

microscale. Yu., *et al.* investigated NiB alloys deposited by electrodeposition and achieved the nano crystallization which has shown improved corrosion resistance compared to amorphous NiB alloys.[6]

Nickel tungsten alloys are reported for improved mechanical properties such as improved tensile strength and hardness properties. Similarly, various other properties such as electrical and tribological properties have also been reported.[7-8] Andrzej, *et al*. investigated the corrosion resistance as a function of W content variation. They did not observe a trend in corrosion resistance with an increase or decrease in tungsten content and hence reported that corrosion resistance varies with the deposition conditions and does not depend on the increase in tungsten content.[9] Studies have been carried out on tungsten concentration with an increase in the wear resistance and even due to the presence of heavy metal, cracking of the surface has been reported.[10] Therefore, nickel tungsten-based materials are used in various fields such as the automobile, aerospace, energy and petroleum industries owing to their high corrosion resistance and wear resistance properties.[11-13]

Nickel tungsten alloys prove to have high corrosion resistance and wear resistance, but there are questions about the material structural uniformity; therefore, to improve the structural properties research group has employed using various Ni-W-X composite protective coatings. Various metal matrices are doped along with alloys such as titanium dioxide, silicon carbide, boron nitride, silicon dioxide, and Carbon Nanotubes (CNTs).[14-19] Similarly, other methods of structural uniformity without cracks can be achieved through treatment methods such as annealing, and shock wave exposure. Shock waves are widely used in various industries such as medicine,[20 - 24] aerospace, and materials testing.

Shock wave exposure is a nonlinear process that changes the mechanical and structural properties of a material. The enhancement of materialistic properties has been researched by various groups. Rita,[25] *et al*., demonstrated copper oxide nanoparticle characteristics change upon exposure to shock waves and proved that the material was structurally stable upon exposure, but morphological changes were observed.[25] Brontvein, *et al.,* synthesised single-faced MoS_2 monocrystalline from MoO_3; usually studies mentioned the difficulty in achieving the monocrystalline phase and this method of shock wave suggested the synthesis of new nanostructures from other layered materials.[26-32]

This group proved the significance of shock waves in the growth of nanocrystalline single-crystal structures. Cui, *et al.*, demonstrated that the growth of SiC nanoparticles on an Al layer, improved the Nano-hardness and wear properties after laser shock-wave-driven nanoparticle implantation. The XRD showed the implanted SiC in the Al layer and the TEM images showed an increased grain size.[33] Therefore, shock waves were proven to have an impact on material properties. Based on the background literature above, this work aims to improve the mechanical and tribological properties of materials. In order to check the effect of bath `temperature variation on structural and mechanical properties of NiW coatings, we have selected to synthesis the coatings at two different temperatures. In connection with that we decided to choose the low temperature (35 ^{0}) and high temperature (75). The variation observed in the properties of NiW coatings also reported in the manuscript.

2. MATERIALS AND METHODS

2.1 Experimental

NiW coatings are electrodeposited on copper substrates using relevant precursors with constant pH at different temperatures. The current density of the electrolyte was maintained at 1 A/dm^2. A copper plate of 7 cm in length and 1.5 cm in breadth was used as the cathode and stainless-steel plate of the same dimension was used as the anode. Both plates were initially cleaned with a soap solution and dipped into H_2SO_4 (10 %) for 3 min. Before electrodeposition, the cathode and anode electrodes were rinsed well with distilled water. Masking of the copper plate was performed with adhesion tape; except for the desired area of the coating. NiW coatings were coated on copper substrates at 35 °C and 75 °C by dipping in an ammonium citrate bath with pH and current density kept constant[34] and the composition was maintained as mentioned below in Table 1.

Table 1. Composition of the precursor solution

Chemicals used	Weight(g)
Nickel sulfate	6
Sodium Tungstate	3
Binder and adhesive	1

XRD analyses were performed for the as-deposited and shock wave-exposed samples at two different temperatures using computer-controlled X'Pert Pro (XRD5). An X-Ray diffractometer employing Cu K_α and K_β radiation was used for the analysis. The scanning was carried out using the θ–θ scan coupling mode; the rating began at 45 KV, and 30 mA. The thickness of the deposited films was measured through gravimetric analysis and was calculated to be ~120 µm. FESEM and EDS analyses were performed for all deposited and exposed conditions. Electrochemical responses such as impedance and the polarisation of the as deposited and shock wave exposed NiW coatings in the presence of a corrosive environment were studied using an electrochemical workstation instrument, the AUT85675 model. The experiments were performed using a three-electrode system. In the present investigation, a platinum electrode and Saturated Calomel Electrode (SCE) were used as the auxiliary and reference electrodes, respectively. Metal specimens coated with NiW at temperature variance and shock wave exposure were used as the working electrodes. During the experiment, the specimen under investigation was dipped in the electrolyte solution, which acted as a corrosive environment for the target metal with NiW coatings. Wear rate analysis was performed for as-deposited and exposed samples with varying wear load using the pin-on-disk method. The hardness of all deposited films was measured using Vickers hardness indenter.

2.2 Shock Wave Exposure

The shock tube of 50 mm ID and 7 m total length is separated into two parts by a diaphragm and a 2-meter driver section, 5 meters driven section as shown in Fig. 1. A high-

pressure source with suitable open/closed valves supplies air to the driver section gradually, with all the connecting flanges and diaphragm airtight. The driven section may be connected to a vacuum pump to maintain the required vacuum pressure.

Figure 1. Photograph of the shock tube experimental facility.

Two highly sensitive pressure transducers (ICP 113B22) that can respond to very rapid pressure hikes are fixed in the driven section at 1.10 m distance between them. These pressure sensors were connected to the NI USB-6356 model data acquisition system through a signal conditioner. The Supply of high-pressure air to the driver section by opening the flow control valve increases the pressure difference on either side of the diaphragm. The diaphragm explodes at a particular pressure difference depending on its strength, producing a shock wave traveling toward the other end of the driven tube.

The two pressure sensors experienced a sudden pressure hike due to the movement of the shock wave as shown in Fig. 2. In which P/P_0 is plotted against the time of observation, where P is the instantaneous static pressure measurement of sensors (1 and 2) and P0 is the initial pressure in the driven tube. It is the plot obtained when the diaphragm of Aluminum material is used as detailed in Table 2. The P/P_0 value is unity until the sensors encounter a shock wave that is propagating along the axial direction of the driven tube. Sensor 1 encounters shock at 0.001 seconds, the instant at which its value rises to approximately 8. Subsequently, sensor 2 encounters the shock wave at 0.00242 seconds and measures the rise in pressure ratio to the same value, so that the time interval between the pressure rises is 0.002391 – 0.001 = 0.001391 seconds.

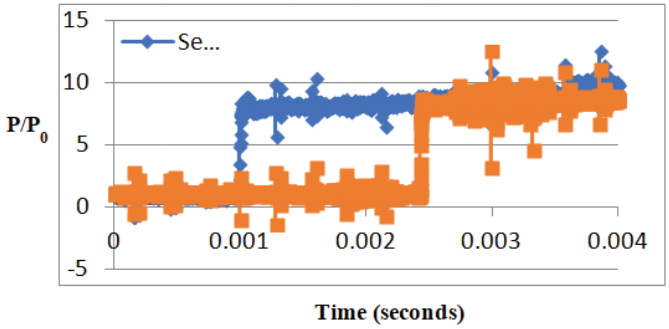

Figure 2. Shock wave pressure characteristics.

divided by the time interval between the recorded hikes, gives rise to the velocity, and hence the Mach number of the shock wave propagating in the driver section. The estimation of the Mach number for two different diaphragms is presented in Table 2.

Table 2. Description of the diaphragm used and the Mach number

Diaphragm Material	Thickness	Velocity (m/s)	Mach Number
Teflon	0.3 mm	454	1.34
Aluminum	1.5 mm	791	2.33

The specimen of investigation is fixed at the closed end of the driven section within the shock tube in such a way that the shock wave traversing through the shock tube will impinge on it. Due to shock impingement, the sample tended to undergo mechanical surface treatment, which is expected to cause structural and morphological changes.

3. RESULTS AND DISCUSSION

3.1 Structural Characteristics

XRD result confirms the existence of FCC (Face Centred Cubic) crystalline phase according to the JCPDS (Joint Committee on Powder Diffraction Standards) card no: (96-152-3163) in all the synthesised NiW coatings except as-deposited thin film at 35 °C.[35] It was observed that the film-coated at 35 °C exhibited the mixed crystalline phase of FCC and hexagonal and also there are no defect peaks seen in the XRD pattern. In the powder XRD analysis, the crystalline size was calculated using Scherrer's formula ($D = (0.9\ \lambda)/(\beta \cos\Theta)$). Where λ – Wavelength of X rays used for the analysis (1.5 Å), β – Ful width half maximum value obtained from XRD peaks. In the prepared polycrystalline materials, the crystalline size referred to every single crystal of NiW coatings.

In comparison with the As-deposited and shockwave-exposed samples as shown in Fig. 3, there is a shift observed in the complete spectrum as a result of increased strain in the as-deposited samples. The strain of the NiW coatings decreases with the increase in the shock wave pressure. Similarly, the deposition temperature also plays an important role to decide the strain and dislocation factors.[36] The strain and dislocation density were decreased while increasing the electroplating bath temperature. However, considering the crystallite size variation with increasing deposition temperature, the crystallite size increases as a phenomenon of abrupt nucleation occurring at higher temperatures as shown in Table 3.

According to the calculated values, the as-deposited samples have smaller particle sizes compared to shock-wave-exposed samples; upon exposure of samples to shock waves, the particles tend to agglomerate with each other forming larger particles. With an increase in the cycle of shock waves, the crystallite size is increased further. The increase in crystallite size contributed to reduced dislocation density and strain. As depicted in figure 3, the peak shift is lower for samples B (Mach number 1.18) and D (Mach number 2.33). Therefore, the crystalline size is inversely related to the strain and dislocation density in this study.

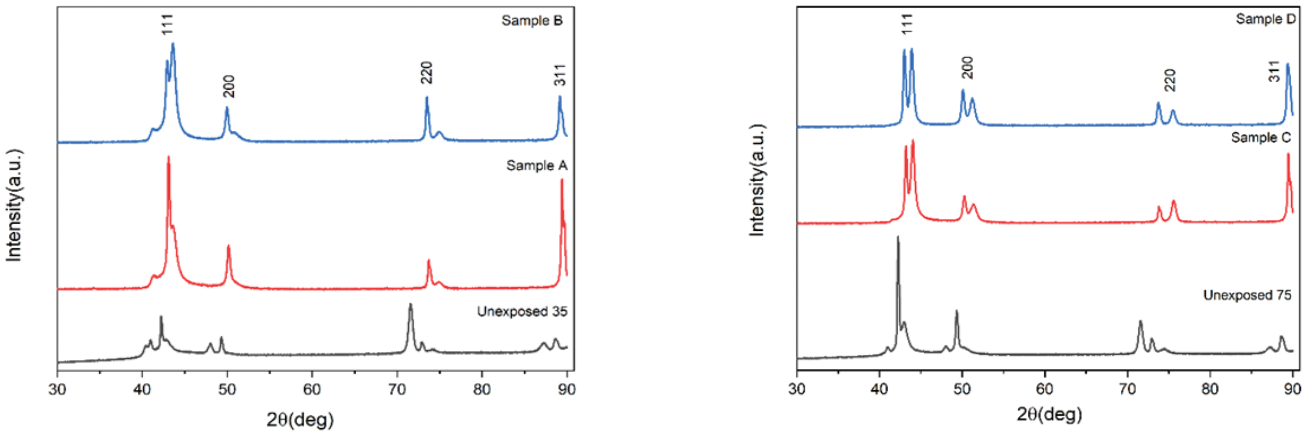

Figure 3. (a) XRD profile – 35 °C-As deposited and shock wave exposed sample and (b) XRD profile – 75 °C-As deposited and shock wave exposed sample.

Table 3. XRD structural characteristic value

Exposure	Crystallite size D (nm)	Dislocation density (nm^{-2})	Strain
As deposited (35 °C)	5.85	0.0292	0.0162
A (35 °C)	7.40	0.0183	0.0125
B (35 °C)	10.00	0.0099	0.0093
As deposited (75 °C)	8.75	0.0132	0.0108
C (75 °C)	16.40	0.0037	0.0056
D (75 °C)	17.33	0.0033	0.0053

3.2 Morphological and Compositional Characteristics

All the as deposited and shock wave exposed NiW coatings were subjected to the FESEM analysis (ZEISS Sigma 300 model) as shown in Fig. 4 (Sample A to D). At 35 °C, deposited NiW coatings showed the micro-cracks and exhibit the nanostructured plate-shaped particles. Furthermore, upon exposure to shock waves, the cracks were reduced at low-pressure and in high-pressure exposure conditions, cracks were not present due to the agglomeration of nanostructured particles. At 75 °C, the as-deposited NiW coating shows crack-free film due to the reorientation of particles which initiates the sudden nucleation at higher bath temperature. Upon exposure to shock waves at lower pressure conditions, the morphology of NiW coatings changed into upright plate-shaped structures due to agglomeration. Similarly, under higher pressure exposure conditions with an increased Mach number, the morphology changed from upright plates into rod-shaped structures. NiW particles undergo changes in various properties such as strain,

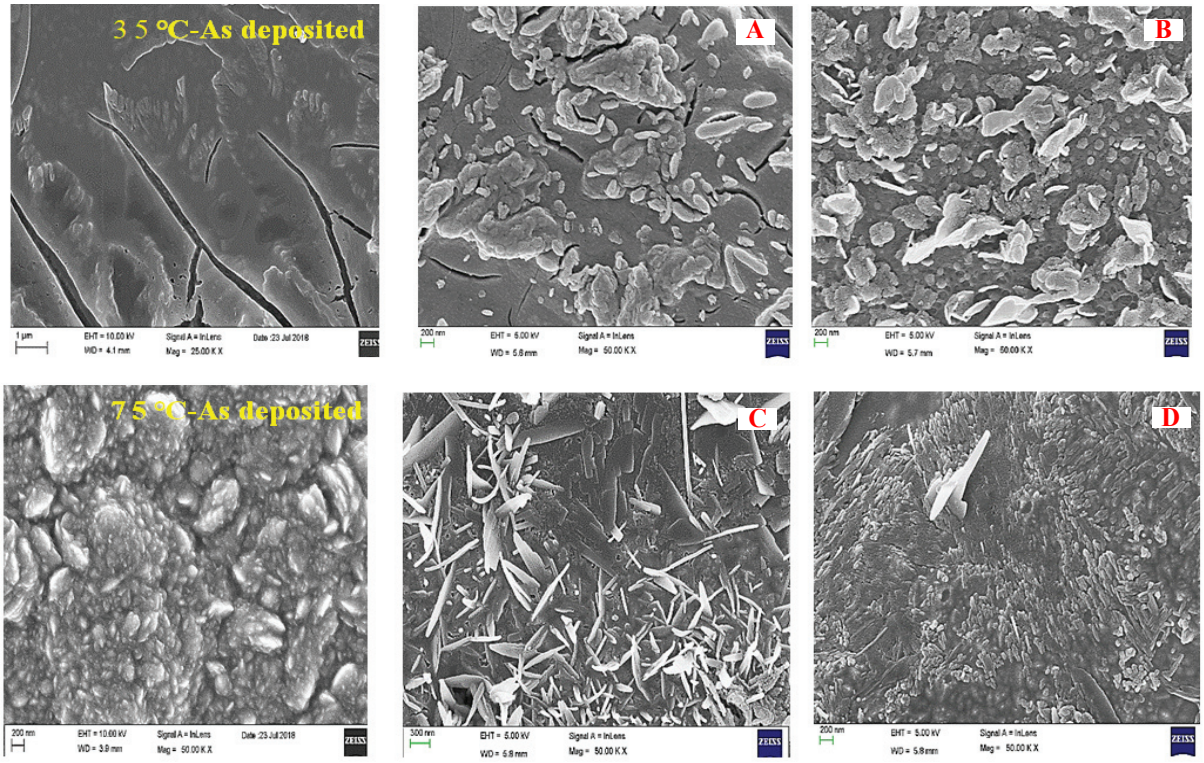

Figure 4. FESEM images of As deposited and shock wave exposed samples.

dislocation density and the particle becomes traumatized and agglomerated thereby increasing the particle size of the film as observed in XRD.[25] Although the particles are agglomerated, the particles show highly resolved boundaries.

The particle size was compared with FESEM study, but after exposing the shock waves, the particles are agglomerated to each other and lead to forming the sheet-like structure.

The chemical composition of the as-deposited and shock-wave exposed NiW coatings were measured using an analysers (Bruker Nano GmbH Berlin, Germany Esprit 1.9). The nickel-tungsten bi-alloy is expected to have a ratio of 85:15 atomic percentage under general conditions. The obtained atomic percentages are listed in Table 4. As expected, the mapping images indicated that nickel was more abundant than tungsten. The sample was coated at a low temperature (35 °C), the shock wave exposed sample shows an increased composition of nickel atomic percentage compared to tungsten. With an increase in the shock wave with a higher mac number, there is the least change in Ni compositional percentage, but in the case of the sample prepared at a higher temperature, there is no compositional variation compared to the shock wave exposed and as-deposited samples. Therefore, it is concluded that the compositional variation upon exposure to high and low-pressure shock waves is observed to be negligible which in turn shows the higher degree of adherence for the deposited coatings with the substrate.

3.3 Wear Analysis

The wear rate was calculated using the Archard equation as shown below

$$V = K\frac{P}{H}$$

where, V is the volumetric wear rate, K is the wear coefficient, P is the applied load, and H is hardness of the material.[37] The calculated wear rate is tabulated as below in Table 5.

As deposited coatings were subjected to 30 N load for wear analysis. The wear rate decreases with an increase in the electrodeposition bath temperature. The measurement of low temperature, as a deposited sample is 285 and for a high-pressure shock wave, the exposed sample is 390. Similarly, for the high-temperature, as deposited coating, the hardness value is 385 and shock wave exposed film showed 425. The hardness value increased with the shock wave exposure. The boiling point of Ni and W is 3186 K, 5828 K respectively and the metal-based alloys upon the increase in temperature lead to thermal expansion. In this present case of NiW binary alloy, the W boiling point is higher than that of Ni. Therefore upon the increase in W content, the thermal expansion of the alloy decreases which leads to the higher hardness of the NiW alloy.

A relation between hardness and wear rate shows that the wear rate is inversely proportional to hardness; therefore, with an increase in hardness, the wear rate decreases.[38] This relationship is depicted by the Archard equation

Table 5. Wear rate calculation and analysis

Sample temp.	Wear coefficient ($mm^3\ N^{-1}\ m^{-1}$)	Wear rate ($mm^3\ m^{-1}$)	Hardness (VH)
35 °C (30N)	0.0001091	$1.15*10^{-5}$	285
75 °C (30N)	0.0001253	$9.76*10^{-6}$	385

3.4 Corrosion Analysis

Electrochemical Impedance (EIS) experiments were performed at an open-circuit potential between frequencies 0.1 Hz and 10 kHz with an amplitude of 10 mV. Polarization plots were obtained by sweeping the voltage between -20 and -200 mV at a scan rate of 1 mV/s. The Nyquist and the Tafel plots were obtained from the electrochemical response. The charge transfer resistance (R_{ct}) values were calculated from the EIS measurements. Tafel polarization analysis was performed by extrapolating the cathodic and anodic curves to the applied potential to obtain the corrosion current densities. The corrosion potential (E_{corr}), corrosion current density (I_{corr}), and polarization resistance (R_p) were extracted from the Tafel plots. The cathodic and anodic slopes of the Tafel plots β_a and β_c were also recorded from the Tafel plots.

The resultant Tafel plots for as-deposited and shock wave-exposed samples were analyzed and the values of corrosion rate and polarisation resistance are tabulated in Table 6. The corrosion rate of as deposited and shock wave exposed samples are compared. The corrosion rate at lower temperature conditions in low-pressure shock wave exposure shows an

Table 4. Compositional analysis of as-deposited and shock-wave exposed samples

Temp. condition	Exposure	Element	Atomic number	Series	Atomic composition [%]
35 °C	As deposited	Ni	28	K Series	83.79
		W	74	L Series	16.21
	Sample A	Ni	28	K Series	85.81
		W	74	L Series	14.19
	Sample B	Ni	28	K Series	90.01
		W	74	L Series	9.99
75 °C	As deposited	Ni	28	K Series	86.09
		W	74	L Series	13.91
	Sample C	Ni	28	K Series	86.04
		W	74	L Series	13.96
	Sample D	Ni	28	K Series	86.99
		W	74	L Series	13.01

increase in corrosion resistance by 6218.9 Ω which is due to the increase in particle size as observed in FESEM and the threshold capacity of the corrosion resistance is reached at an intermediate point between the applied pressure range, owing to which a reduction in corrosion resistance is observed. At higher temperature conditions, the sample exposed to lower pressure compared to the as-deposited sample, the corrosion resistance increased by a range difference of 134.6 Ω and at higher pressure conditions increased by an appreciable amount of 18380.3 Ω. Compared to the as-deposited sample, the higher pressure condition exposed sample D has more corrosion resistance and thereby higher temperature conditions exposed samples are more resistant to corrosion as the morphology is rod-shaped and compositional data is stable.

The semicircle in the Nyquist plots shows that the deposition of nickel tungsten on the copper plate is a charge transfer reaction that controls the corrosion process. By comparing both the plots in Fig. 5(b) the coated alloys at low temperature and high temperature have similar single capacitive loops; hence these systems did not alter redox reactions irrespective of the temperature. The diameter of the semicircle is a measure of electron transfer across the exposed area of the metal surface and it is inversely proportional to the rate of corrosion. In the impedance graph, the shock-wave-exposed samples have higher corrosion resistance when compared to the unexposed samples. Complementing the Tafel graph values, the Nyquist plot shows higher corrosion resistance for sample D followed by samples A, B and C. Sample A should exhibit better corrosion resistance than sample B because, upon high-pressure shock wave exposure, the particle agglomeration increases and the structural, and morphological changes are observed accordingly which produces the reduction in corrosion rate. As the nanostructured particles get agglomerated to form microstructural particles, a higher rate of electron transfer is observed for sample D.

Upon shock wave exposure to the NiW alloy in various pressure conditions, their mechanical properties like hardness have been increased due to the agglomeration of NiW particles which intern enhances the corrosion resistance value without any appreciable compositional changes.

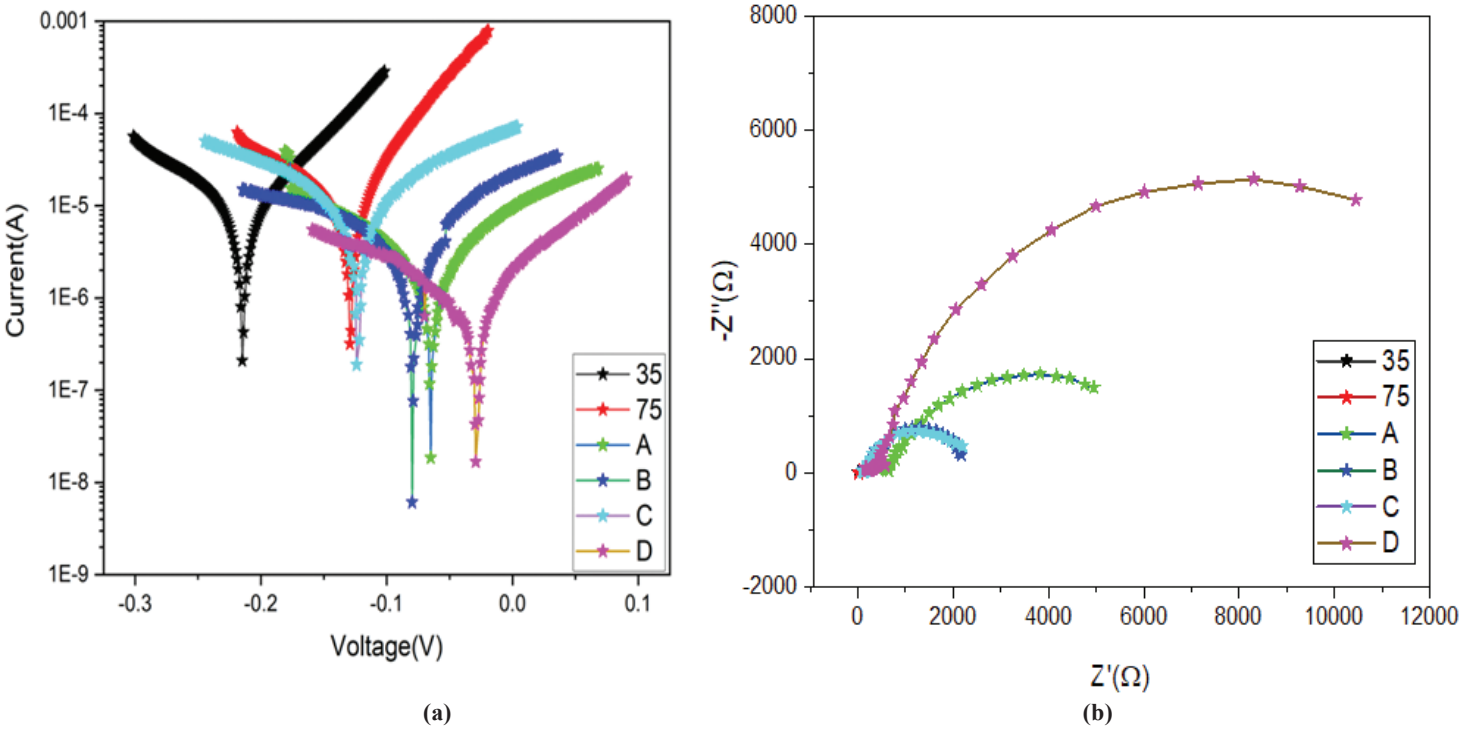

(a) (b)

Figure 5. Corrosion analysis (a) Tafel plot and (b) Nyquist plot.

Table 6. EIS analysis corrosion resistance calculation

ss	Sample name	$E_{corr, Calc}$ (V/cm²)	$E_{corr, Obs}$ (V/cm²)	i_{corr} (A/cm²)	Polarization resistance (Ω/cm²)
	As deposited	-0.2148	-0.2145	1.7E-05	1775.3
35°C	A	-0.0831	-0.0655	7.32E-06	7989.2
	B	-0.0846	-0.0809	3.76E-05	5405.8
	As deposited	-0.1286	-0.1288	8.25E-7	2130.1
75°C	C	-0.1249	-0.1231	5.79E-05	2264.7
	D	-0.0226	-0.0295	1.62E-06	20645

4. CONCLUSION

The NiW protective coatings were exposed to shock waves with varying Mach numbers (high and low pressure). The structural analysis performed using XRD showed a single cubic structural growth in the shock-wave-exposed samples compared to the as-deposited samples, which explains the stability of the protective coating. The crystalline size of the shock wave-exposed samples was larger than that of as-deposited samples, which is evident in the FESEM image of particle agglomeration upon shock wave exposure. The wear rate analysis was performed on the as-deposited samples and showed a low wear rate on the high-temperature deposited samples as the hardness of the samples was increased. The corrosion rate of the NiW sample coated at high temperature and exposed to high pressure was reduced to an appreciable amount. Therefore, upon shock wave exposure, the coating properties are structurally and mechanically enhanced.

REFERENCES

1. Nasirpouri, F.; Alipour, K.; Daneshvar, F. & Sanaeian, M. R. Electrodeposition of anticorrosion nanocoatings. In Corrosion Protection at the Nanoscale, edited by Susai Rajendran, Tuan ANH Nguyen, Saeid Kakooei, Mahdi Yeganeh, Yongxin Li, Elsevier, 2020, 473-497..
2. Xu, J.; Wiese, G.; John, H.; & Liu, X. Oil-Grade Alloy 718 in Oil Field Drilling Applications. In Proceedings of the 7th International Symposium on Superalloy 718 and Derivatives TMS: The Minerals, Metals and Materials Society, edited by Pittsburgh, PA, USA, 2010, 521-537.
3. Gopala Rao Thellaputta, Pulcharu Subhash Chandra, & C.S.P. Rao. Machinability of Nickel Based Superalloys: A Review. *Mater. Today*: *Proc*, 2017, **4**(2), 3712-3721. doi:10.1016/j.matpr.2017.02.266
4. Srivastava, M.; Selvi, V.E.; Grips, V.W. & Rajam, K.S. Corrosion resistance and microstructure of electrodeposited nickel–cobalt alloy coatings. *Surf. Coat. Technol.* 2006, **201**(6), 3051-3060. doi: 10.1016/j.surfcoat.2006.06.017
5. Allahyarzadeh, M.H.; Aliofkhazraei, M.; Rezvanian, A.R.; Torabinejad, V & Rouhaghdam, A.S. Ni-W electrodeposited coatings: characterization, properties and applications. *Surf. Coat. Technol*., 2016, **307**, 978-1010. doi: 10.1016/j.surfcoat.2016.09.052
6. Yu, N.; Bekish Poznyak S.K.; Tsybulskaya, L.S. & Gaevskaya, T.V. Electrodeposited Ni–B alloy coatings: Structure, corrosion resistance, and mechanical properties. *Electrochim. Acta*, 2010, **55**(7), 2223-2231. doi:10.1016/j.electacta.2009.11.069
7. Sriraman, K.R; Ganesh Sundara Raman, S & Seshadri, S.K. The corrosion behavior of electrodeposited nanocrystalline Ni–W and Ni–Fe–W alloys. Mater. *Sci. Eng*., A, 2007, 460–461, 39-45. doi:10.1016/j.msea.2007.02.055
8. Eliaz, N.; Sridhar, T.M & Gileadi, E. Synthesis and characterization of nickel tungsten alloys by electrodeposition. *Electrochim. Acta*, 2005, **50**(14), 2893-2904. doi: 10.1016/j.electacta.2004.11.038
9. Królikowski, A.; Płońska, E.; Ostrowski, A.; Donten, M. & Stojek, Z. Effects of compositional and structural features on corrosion behavior of nickel–tungsten alloys. *J. Solid State Electrochem.,* 2009, **13**, 263–275. doi: 10.1007/s10008-008-0712-2
10. Yamasaki, T.; Schloβmacher, P.; Ehrlichand, K. & Ogino, Y. Formation of amorphous electrodeposited Ni-W alloys and their nanocrystallization. *Nanostruct. Mater*., 1998, **10**(3), 375–388. doi:10.1016/S0965-9773(98)00078-6
11. Chianpairot, A.; Lothongkum, G.; Schuh, C.A. & Boonyongmaneerat, Y. Corrosion of nanocrystalline Ni–W alloys in alkaline and acidic 3.5 wt.% NaCl solutions. *Corros. Sci*., 2011, **53**, 1066–1071. doi: 10.1016/j.corsci.2010.12.001
12. Yin, Z.F.; Zhao, W.Z.; Lai, W.Y. & Zhao X.H. Electrochemical behavior of Ni-base alloys exposed under oil/gas field environments. *Corros. Sci.*, 2009, **51**, 1752–1756. doi: 10.1016/j.corsci.2009.04.019
13. Lee, D.B.; Ko, J.H. & Kwon, S.C. High-temperature oxidation of Ni–W coatings electroplated on steel. *Mater. Sci. Eng. A*., 2004, **380**, 73–78. doi: 10.1016/j.msea.2004.03.036
14. Arunsunai Kumar, K.; Paruthimal Kalaignann, G. & Muralidharan, V.S. Direct and pulse current electrodeposition of Ni–W–TiO_2 nanocomposite coatings. *Ceram. Int.*, 2013, **39**, 2827–2834. doi: 10.1016/j.ceramint.2012.09.054
15. Goldasteh & Rastegari, S. The influence of pulse plating parameters on structure and properties of Ni–W–TiO_2 nanocomposite coatings, *Surf. Coat. Technol.,* 2014, **259**, 393–400. doi: 10.1016/j.surfcoat.2014.10.064
16. Yao, Y.; Yao, S.; Zhang, L. & Wang, H. Electrodeposition and mechanical and corrosion resistance properties of Ni–W/SiC nanocomposite coatings. *Mater. Lett.*, 2007, **61**, 67–75. doi: 10.1016/j.matlet.2006.04.007
17. Sangeetha, S. & Kalaignan, G.P. Tribological and electrochemical corrosion behavior of Ni–W/BN (hexagonal) nanocomposite coatings. *Ceram. Int*., 2015, **l9**, 10415-10424. doi: 10.1016/j.ceramint.2015.04.089
18. Fan, Y.; He, Y.; Luo, P.; Shi, T. & Li, H. Pulse current electrodeposition and characterization of Ni-W-MWCNTs nanocomposite coatings. *J. Electrochem. Soc.,* 2015, **162**(7), D275-D274. doi: 10.1149/2.0391507jes
19. Sassia, W.; Dhouibi, L.; Bercot, P. & Rezrazi, M. The effect of SiO_2 nanoparticles dispersion on Physico-chemical properties of modified Ni–W nanocomposite coatings. *Appl. Surf. Sci.,* 2015, **324**, 369–379. doi: 10.1016/j.apsusc.2014.10.142
20. Rassweiler, J.J.; Knoll, T.; Köhrmann, K.U.s; Mc Ateer, J.A; Lingeman, J.E; Cleveland, R.O; Bailey, M.R. & Chaussy, C. Shock wave technology and application: an

update. *Eur Urol*. 2011, 59(5), 784-796.
doi: 10.1016/j.eururo.2011.02.033

21. Nitin, P.; Wasekar Anthony, P.; O'Mullane, Md Abu Sayeed & Sundararajan, G. Influence of SiC reinforcement content and heat treatment on the corrosion behavior of pulsed electrodeposited Ni-W alloy metal matrix composite. *Materialia*, 2022, **22**, 101390. doi: 10.1016/j.mtla.2022.101390.
22. Sriraman, K.R; Ganesh Sundara Raman, S & Seshadri, S.K. Synthesis and evaluation of hardness and sliding wear resistance of electrodeposited nanocrystalline Ni–W alloys. *Mater. Sci. Eng.A,* 2006, **418**(1–2), 303-311. doi: 10.1016/j.msea.2005.11.046
23. Nitin, P.; Wasekar ; Lavakumar Bathini, L.; Ramakrishna, D.; Srinivasa, Rao & Padmanabham, G. Pulsed electrodeposition, mechanical properties and wear mechanism in Ni-W/SiC nanocomposite coatings used for automotive applications. *Appl. Surf. Sci.,* 2020, **527**, 146896. doi: 10.1016/j.apsusc.2020.146896
24. Pramod Kumar, U.; Shanmugan, S.; Joseph Kennady, C. & Shibli, S.M.A. Anti-corrosion and microstructural properties of Ni-W alloy coatings: effect of 3,4-Dihydroxybenzaldehyde. *Heliyon.* 2019, **5**(3), 01288. doi: 10.1016/j.heliyon.2019.e01288.
25. Rita, A.; Sivakumar, A. & Martin Britto Dhas, S.A. Influence of shock waves on structural and morphological properties of copper oxide NPs for aerospace applications. *J. Nanostruct. Chem.,* 2019, **9**, 225–230. doi: 10.1007/s40097-019-00313-0
26. Brontvein, O.; Jayaram, V.; Reddy, K.P.J; Gordon, J.M & Tenne, R.: Two-step synthesis of MoS_2 nanotubes using shock waves with lead as a growth promoter. Z. Anorg. *All. Chem.* 2014, **640**, 11152– 11158. doi: 10.1002/zaac.201300329
27. Indyka, P.; Beltowska, E.L.; Tarkowskib, L.; Bigosb, A. & Garcia-Lecinac, E. Structure characterization of nanocrystalline Ni–W alloys obtained by electrodeposition. *J. Alloys Comp.,* 2014, **590**, 75-79. doi: 10.1016/j.jallcom.2013.12.085
28. Shreeram, D.D.; Li, S; Bedekar, V.; Cong, H & Doll G.L. Effect of reverse pulse time on electrodeposited Ni-W coatings. *Surf. Coating. Technol.,* 2017, **325**, 386–396. doi:10.1016/J.SURFCOAT.2017.06.037
29. Salehikahrizsangi, P.; Raeissi, K.; Karimzadeh, F.; Calabrese, L. & Proverbio, E. Effects of surface morphology on erosion–corrosion and corrosion resistance of highly hydrophobic nickel-tungsten electrodeposited film. *Coatings.,* 2021, **11**(9), 1084. doi: 10.3390/coatings11091084
30. Pao-Chang, Huang; Chih-Cheng, Chou; Han-Tao, Wang; Chun-Hao, Cheng; Kung-Hsu, Hou & Ming-Der, Ger. Tribocorrosion study of electrodeposited NiW alloy/BN(h) composited coatings for piston rings. *Surf. Coating. Technol.,* 2022, **436**, 128289. doi: 10.1016/j.surfcoat.2022.128289.
31. Baosong, Li; Dandan, Li; Tianyong Mei; Wenzhe Xia & Weiwei Zhang. Fabrication and characterization of boron nitride reinforced Ni–W nanocomposite coating by electrodeposition. *J. Alloys Compd.,* 2019, **777**, 1234-1244. https://doi.org/10.1016/j.jallcom.2018.11.081.
33. Thirumalesh, K.; Somashekharappa, H.M.; Raju, S.P. & Swaroop, K. Study on effects of shockwave treatment on PVA films in view of electrical property changes. *Mater. Res. Express* 2020, **7**, 015344. https://doi.org/10.1088/2053-1591/ab6ca1
34. Chengyun, Cui; Xigui, Cui; Xiaodong, Li; Kaiyu, Luo; Jinzhong, Lu; Xudong, Ren; Jianzhong, Zhou; Cui, Fang; Raif, Farkouh & Yongfeng, Lu. Plastic-deformation-driven SiC nanoparticle implantation in an Al surface by laser shock wave: Mechanical properties, microstructure characteristics, and synergistic strengthening mechanisms. *Int. J. Plast.,* 2018, **102**, 83-100. doi: 10.1016/j.ijplas.2017.12.004
35. Kannan, R. & Kokila, S. Synthesis and structural characterization of CoNiW alloy thin films by electrodeposition. *Int. J. Thin Fil. Sci. Tec.,* 2015, **4**(1), 59-62. doi: 10.12785/ijtfst/040111
36. Kalaiarasi, S.; Sivakumar, A.; Martin Britto Dhas S.A. & Jose, M. Shock wave-induced anatase to rutile TiO_2 phase transition using pressure-driven shock tube. *Mater. Lett.,* 2018, **219**, 72-75. doi: 10.1016/j.matlet.2018.02.064

ACKNOWLEDGEMENT

This work is a part of the project fully sponsored by DRDO ARMREB. The authors are thankful for the financial support extended from DRDO ARMREB (ARMREB/MAA/2020/227).

CONTRIBUTORS

Ms G. Nivetha received her BTech (Nanotechnology) from SRM Institute of Science and Technology and MTech (Nanotechnology) from Vellore Institute of Technology. Currently, she is working as JRF in DRDO ARMREB funded project in Kumaraguru College of Technology. Her area of specialisation is surface coatings using electrodeposition technique, spray pyrolysis deposition, ion beam sputtering and in characterisation hands-on experience in AFM machining, analysis of the XRD spectrum using match software. In this paper, she planned the experiments, analysed the structural, morphological, mechanical behaviour and prepared the manuscript.

Dr R. Kannan received PhD from Anna University. He is currently working at Kumaraguru College of Technology as an Assistant Professor. He is also the Principle Investigator of the DARMREB-funded project. His area of specialisation is surface coatings of metal alloy through the electrodeposition technique. He has technical research articles published in national, international journals and conference proceedings.
In this paper, He has guided the author through deposition, result compilation, result interpretation and reviewed the manuscript.

Mrs M. Selvambikai obtained her MSc degree from Madurai Kamaraj University, MPhil from Bharathidasan University and MTech from

Anna university. She is currently working as Assistant Professor in Physics at Kumaraguru College of Technology, Tamilnadu. Her area of specialisation are materials science and remote sensing. She is actively doing the materials science research projects like synthesis and characterization of refractory metal-based thin films for various industrial applications. She has published several research papers in peer-reviewed international journals.
In this paper, she has been involved to prepare and review the manuscript.

Prof. C. Vasantharaj is presently working as Director of Kumaraguru Centre for Industrial Research & Innovation (KCIRI) in Kumaraguru College of Technology, Coimbatore. Prior to taking up his role at Kumaraguru College of Technology, he served as the Vice President at Cades Digitech Pvt Ltd., Bangalore, where he was responsible for India-Defence business and program management of all defence projects of the company.
He also served as Project Director at the Centre for Airborne Systems, DRDO, Bangalore, where he monitored and coordinated the project activities at all work centres developing various AEW&C systems. He was also involved in the successful development of PINAKA rocket system and Integrated Material Management System, IMMS at ARDE, Pune.
In this paper, he has guided the author for reviewing the manuscript.

Dr Praveen Kumar B. is currently working as Scientist in DRDO-ARDE Pune. His current research interests are: Processing and characterization of advance functional materials, porous ceramics, pulse power generators and sensor devices. He earned his BE from NIT Trichy and PhD from IIT Madras, in the field of sensor materials and devices. He has published about 50 research papers in peer-reviewed journals and about 18 papers in conference proceedings. He is recipient of DRDO Young Scientist Award, DRDO Technology Group Award and Distinguished Young Alumni Achiever Award- NIT Trichy.
In this paper, he has guided the author and reviewed the manuscript.

Dr Premkumar P.S. completed Bachelor of Engineering in Aeronautical in Bharathiar University, Coimbatore & pursued MS (By Research) in Aerospace Engineering in Madras Institute of Technology (MIT), Anna University, Chennai. He is holding PhD in Aerospace Engineering from MIT, Anna Univesity, Chennai in the area of Propeller Aerodynamics. He is having 19 + years of experience in the area of Experimental & Computational Aerodynamics. Currently he is working as Associate Professor in the Aeronautical Engineering department of KCT. He has 30+ international journal & conference publications in his credit. He has completed one UGC Minor Research Project and two DRDO CARS (DRDL, Hyderabad & ADE, Bangalore) and one DRDL CARS project is in progress.
He has contributed in this paper for shock tube testing of the specimens.

Dr Sundararaj K. obtained his MTech in Aerospace Engineering from IIT Madras and PhD from Anna University, Chennai. He is currently working as Head of the Department of Aeronautical Engineering at Kumaraguru College of Technology, Coimbatore, India. His areas of interest are: Low and high-speed experimental aerodynamics and shock wave boundary layer interactions. He has guided three PhDs in the areas of shock interactions.
In the present work, he guided the author in setting up the shock tube experimental facility.